J. Biophotonics **6**, No. 8, 612–621 (2013) / **DOI** 10.1002/jbio.201200063

Journal of BIOPHOTONICS

FULL ARTICLE

A molecular imaging analysis of Cx43 association with Cdo during skeletal myoblast differentiation

Daniele Nosi[*,1], *Raffaella Mercatelli*[*,2], *Flaminia Chellini*[1], *Silvia Soria*[3], *Alessandro Pini*[1], *Lucia Formigli*[1], *and Franco Quercioli*[**,4]

[1] Dipartimento di Anatomia, Istologia e Medicina Legale, Università di Firenze, Largo Brambilla 3 – Firenze, Italy
[2] Istituto dei Sistemi Complessi, Consiglio Nazionale delle Ricerche, via Madonna del Piano 10 – Sesto Fiorentino, Italy
[3] Istituto di Fisica Applicata Nello Carrara, Consiglio Nazionale delle Ricerche, via Madonna del Piano 10 – Sesto Fiorentino, Italy
[4] Istituto Nazionale di Ottica, Consiglio Nazionale delle Ricerche, Via Nello Carrara 1 – Sesto Fiorentino, Italy

Received 4 April 2012, revised 12 July 2012, accepted 30 July 2012
Published online 30 August 2012

Key words: Förster resonance energy transfer, fluorescence lifetime imaging microscopy, C2C12 myoblasts, myogenesis

Supporting information for this article is available free of charge under http://dx.doi.org/10.1002/jbio.201200063

Cell-to-cell contacts are crucial for cell differentiation. The promyogenic cell surface protein, Cdo, functions as a component of multiprotein clusters to mediate cell adhesion signaling. Connexin 43, the main connexin forming gap junctions, also plays a key role in myogenesis. At least part of its effects is independent of the intercellular channel function, but the mechanisms underlying are unknown. Here, using multiple optical approaches, we provided the first evidence that Cx43 physically interacts with Cdo to form dynamic complexes during myoblast differentiation, offering clues for considering this interaction a structural basis of the channel-independent function of Cx43.

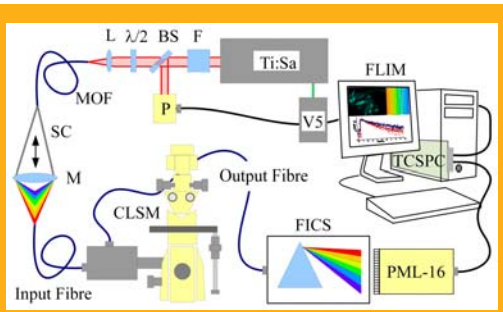

Hyperspectral FLIM FRET setup.

1. Introduction

The study of cell signalling pathways is of particular interest for the identification of specific interactions between proteins and other cellular components. Fluorescence microscopy has become a powerful technique to probe such cellular activity, because it allows the selective and specific detection of molecules at low concentration levels [1]. Intensity images, however, only reveal cellular organization, while functional measurements such as fluorescence lifetime imaging (FLIM) can probe cellular activity and protein interactions in a single cell. For a complete study on cellular activity, a combination of fluorescence measurements is needed: intensity, lifetime, and spectral imaging.

In the recent years much attention has been drawn to the role played by several classes of intercellular junctional proteins and related signaling in the cell-contact-based regulation of myoblast differentiation [2].

Skeletal myoblasts are undifferentiated mononuclear precursor cells which are responsible for postnatal muscle growth and injury-induced muscle regen-

[*] D. Nosi and R. Mercatelli contributed equally to this manuscript
[**] Corresponding author: e-mail: franco.quercioli@ino.it, Phone: + 39 055 5226634, Fax: + 39 055 5226683

eration. Their activation requires re-entry in the cell cycle, expression of muscle-specific transcriptional factors and formation of multinucleated myofibers [3, 4]. There is growing evidence indicating that myogenic differentiation is regulated by signals emanating from sites of adherent and gap junction formation [5, 6]. The adherent junctions are composed by transmembrane adhesion receptors, the cadherins, linked to scaffolding and cytoskeletal elements to form multiprotein clusters, which are capable not only of maintaining the physical cellular linkages and the tissue architecture but also of influencing crucial downstream functions [7, 8]. Of interest, Cdo, a multifunctional cell surface protein with immunoglobulin and fibronectin III, repeats in its ectodomain and a long intracellular region exerts its pro-myogenic action functioning as a component of the cadherin-complexes [9]. This molecule binds to N-cadherin and upon cell cell-cell adhesion, mimicked by N-Cadherin ligation, undergoes activation via interaction with signaling and adaptor proteins, including p38MAPK, thereby initiating intracellular signal transduction cascades which through phosphorylation of substrates, stimulate MyoD-dependent, muscle-specific gene expression [10–13]. It is expressed on muscle precursor cells and developing skeletal muscle and upregulated in differentiating myoblasts by high cell density or serum removal [14]. Its critical role during myogenesis is also revealed by the results showing that mice lacking Cdo exhibit delayed skeletal myogenesis, and Cdo−/− primary myoblasts have defects in myoblast differentiation [15].

Adherens junctions are intimately associated with gap junctions [16, 17], they are formed by hemichannels (connexons), made up by six proteins (connexins) which may oligomerize in monomeric or heteromeric patterns [18]. Two hemichannels assemble in mirror symmetry to form an intercellular bridge among adjacent cells. The close association between adherens and gap junction reflect the requirement of a close membrane-membrane apposition for gap junction formation and function; for instances, in cardiomyocytes, the mechanical support of the adherens junction ensures the propagation through the gap junction of the action potentials along the cardiomyocytes [16, 17]. We have previously shown that connexin 43 (Cx43), the main connexin isoform expressed in skeletal myoblasts, besides forming intercellular channels which regulate the trafficking and functional integration among the adjacent myoblasts, serves a gap-junction independent pro-myogenic function [19]. Indeed, C2C12 myoblasts transfected with a dominant negative Cx43 construct, which although forming functional gap junctions lack the ability to bind to cortical actin, differentiate defectively in culture, further stressing the idea that Cx43 *per se* might be required for some aspects of the connexin-mediated pro-myogenic signaling. Of particular interest are the observations that the carboxyl tail of Cx43 is subjected to phosphorylation by several kinases and can bind several protein and cytoskeletal elements, suggesting that it may play a central role in the control of signalling cascade regulating cell differentiation [20, 21]. However, the mechanisms underlying this function are not known.

On the basis of all these considerations, in the present study we searched for a possible functional interaction between Cx43 and Cdo as a preliminary attempt to expand our knowledge on the biological functions of Cx43 in skeletal myogenesis. By combining different optical microscopic techniques, ranging from confocal immunofluorescence to hyperspectral FLIM-FRET, we showed that Cx43 and Cdo displayed the same spatiotemporal expression pattern and physically interact to form dynamic complexes in C2C12 cells during myogenesis, offering clues for considering this interaction a structural basis of the channel-independent function of Cx43.

Förster Resonant Energy Transfer (FRET) can be an useful tool to study protein-protein interaction by imaging their spatial and temporal dynamics in cells. FRET is a non radiative transfer of energy from an excited state fluorophore (the donor) to a different spatially colocalized fluorophore (the acceptor). In practice, FRET can only be observed for donor-acceptor separations less than 10 nm and is commonly detected with three different techniques: sensitized emission, acceptor photobleaching and FLIM [22]. Among all the techniques, sensitized emission is the easiest one but FLIM is the most reliable one [23]. FLIM determines the fluorescence decay time for each pixel of the acquired image and creates a map of the molecular environment of a fluorophore. FLIM is almost insensitive to intensity artifacts and fluorophores concentration but highly sensitive to local changes in the environment such as variations of pH, physiological ions or interacting partners [22]. Hyperspectral FLIM [24, 25] is a technique allowing simultaneously recording of the full emission spectrum and temporal decay curves of a biological specimen and may be useful for FRET measurements in order to exclude changes in lifetime due to other local variations.

2. Experimental

2.1 Cell preparation and sample staining

Murine C2C12 skeletal myoblasts obtained from American Type Culture Collection (ATCC, Manassas, VA), were grown in Dulbecco's modified Eagle's medium (DMEM) supplemented with 10% fetal

bovine serum (FBS), penicillin (100 U/ml) and streptomycin (100 μg/ml) (Sigma, Milan, Italy) and maintained at 37 °C in a humidified atmosphere of 5% CO_2.

For myogenic differentiation experiments, cells were grown on glass coverslips until 80% confluence and induced to differentiate by switching to differentiation medium (DM), containing 2% horse serum (HS, Sigma) for different times (24, 48 and 72 hours), in the presence or absence of S1P (1 μM, 2 mM stock solution in dimethylsulfoxide, Calbiochem, La Jolla, CA).

C2C12 cells grown on glass coverslips were fixed in 0.5% buffered paraformaldehyde (PFA) for 10 minutes at room temperature. After permeabilization with cold acetone, the fixed cells were blocked with 0.5% Bovine Serum Albumin (BSA) and 3% glycerol in Phosphate Buffer Solution (PBS) for 20 minutes and incubated with mouse monoclonal anti-Cx43 (1 : 250; Millipore, Milan, Italy) and goat polyclonal anti-Cdo (1 : 200; Santa Cruz, Milan, Italy) antibodies over night at 4 °C. The immunoreactions were revealed by incubation with goat anti-mouse Alexa Fluor 568-conjugated IgG (1 : 100; Molecular Probes Inc., Eugene, OR) and rabbit anti-goat Alexa Fluor 488-conjugated IgG (1 : 200; Molecular Probes) for 1 hour at room temperature. Negative controls were carried out by replacing the primary antibodies with nonimmune mouse serum. After washing, the coverslips containing the immunolabelled cells were mounted with an antifade mounting medium (Biomeda Gel mount, Electron Microscopy Sciences, Foster City, CA).

2.2 Confocal imaging

Observations were carried out with a Laser Scanning Confocal Microscope Leica TCS SP5 (Leica Microsystems, Mannheim, Germany) equipped with HeNe and Ar laser excitation sources. The acquisitions were performed using a Leica Plan Apo 63/1.43NA oil immersion objective and differential interference contrast (DIC) optics for transmission imaging.

Once excited by the 488 nm Ar laser line, the Alexa Fluor 488 fluorescence was gathered into the spectral window 500–550 nm and the image green channel was assigned to it. The 543 nm HeNe laser line was used instead to excite the Alexa Fluor 568 whose fluorescence emission was recorded in the spectral window 600–650 nm and assigned to the image red channel.

Series of optical sections (1024 × 1024 pixels each; field size 200 μm, pixel size of about 200 nm) were taken through the depth of the cells at intervals of 370 nm. Images were then Z-projected onto a single 'extended focus' image. The fluorescence Z-projections and DIC images were than merged to localize the immunostaining on the cell surface.

2.3 Western Blotting

Cells were re-suspended in appropriate volume of cold lysis buffer (10 mM Tris/HCl, pH 7.4, 10 mM NaCl, 1.5 mM $MgCl_2$, 1% Triton X-100, 2 mM Na_2 EDTA), added with 10x Sigmafast Protease Inhibitor cocktail tablets (Sigma). Upon centrifugation at 13,000 g for 15 minutes at 4 °C, the supernatants were collected and the total protein content was measured spectrophotometrically using micro-BCATM Protein Assay Kit (Pierce, IL, USA). 50 μg of total proteins were electrophoresed by SDS-PAGE (200V, 1h) using a denaturating 7.6% polyacrylamide gel and blotted onto nitrocellulose membranes (Amersham, Cologno Monzese, Italy; 150 V, 1h). The membranes were blocked with PBS containing 0.1% Tween (Sigma) and 1% bovine serum albumin (AT-PBS) (Sigma) for 1 h at room temperature and incubated overnight at 4 °C with goat polyclonal anti-Cdo antibody (1 : 400 in AT-PBS; Santa Cruz Biotechnology) and rabbit polyclonal anti-Cx43 antibody (1 : 750 in AT-PBS; Santa Cruz Biotechnology). Membranes were also immunostained with rabbit polyclonal anti-β-actin antibody (diluted 1 : 20.000 in AT-PBS; Sigma), assuming β-actin as control invariant protein. After washing with T-PBS (Tween-PBS), the membranes were incubated with peroxidase-labeled anti-goat or anti-rabbit antibodies (1 : 15.000 in AT-PBS; Vector, Burlingame, CA) for 1 hour, at room temperature and the immunoreactivity was detected by the ECL chemiluminescent substrate (Amersham). Densitometric analysis of the bands was performed using Scion Image Beta 4.0.2 image analysis software (Scion Corp.) and the values normalized to β-actin values.

2.4 Colocalization analysis

To verify the initial hypothesis regarding the interaction between cadherin-associated Cdo, stained with Alexa Fluor 488, and Cx43 protein, stained with Alexa Fluor 568, colocalization analysis was carried out on the 3D confocal Z-stacks acquired from double stained samples (Table 1). Though colocalization does not necessarily mean that the two proteins directly interact, it is otherwise true that in the absence of a significant correlation between the spatial distribution of the two biomolecules, it is unlikely that they have a stable interaction [26].

Colocalization analysis was performed by using the JACOP plug-in routine made available for the

Table 1 Description of the samples used for molecular imaging.

Sample	Description
T0	Cdo (Alexa Fluor 488) and Cx43 (Alexa Fluor 568) in C2C12 myoblasts.
DM 24 h	Cdo (Alexa Fluor 488) and Cx43 (Alexa Fluor 568) in C2C12 myoblasts cultured for 24 h in differentiation medium.
DM 48 h	Cdo (Alexa Fluor 488) and Cx43 (Alexa Fluor 568) in C2C12 myoblasts cultured for 48 h in differentiation medium.
DM 72 h	Cdo (Alexa Fluor 488) and Cx43 (Alexa Fluor 568) in C2C12 myoblasts cultured for 72 h in differentiation medium.
DM + S1P 24 h	Cdo (Alexa Fluor 488) and Cx43 (Alexa Fluor 568) in C2C12 myoblasts cultured for 24 h in differentiation medium + 1 μM S1P
Donor control	Cdo (Alexa Fluor 488) in C2C12 myoblasts cultured for 48 h in differentiation medium
Acceptor control	Cx43 (Alexa Fluor 568) in C2C12 myoblasts cultured for 48 h in differentiation medium

ImageJ software (http://rsbweb.nih.gov/ij). Pearson's Correlation coefficient (PC) was chosen for evaluating colocalization levels [27].

2.5 *FRET sensitized emission*

Though colocalization analysis represents a valuable statistical screening test, it is on the other hand well known that a significant correlation does not necessarily mean a real physical interaction between the two molecules. The optical Point Spread Function (PSF) volume, in the order of 1 μm^3, is too wide to state whether two proteins inside it really interact. We then performed FRET analysis (FRET volume is in the order of $10^{-6}\,\mu m^3$) to determine whether Cx43 and Cdo interacted with one another. Alexa Fluor 488 (donor D) and Alexa Fluor 568 (acceptor A) are a good FRET pair, with a Förster radius of 6.2 nm [28].

Sensitized Emission (SE) FRET is one of the most used and simple methods for the evaluation of FRET efficiencies [29]. The method involves measuring the acceptor fluorescence emission when only the donor has been excited (I_{AD}) in sequence with the emission detection of the directly excited acceptor (I_{AA}). The ratio of these two signals is approximately proportional to the FRET efficiency [30]:

$$E \propto \mathrm{SE}/I_{AA} \approx I_{AD}/I_{AA} \qquad (1)$$

The last approximation holds when the spectral bleed-through contributions are negligible. These noise components are mainly of two types: the donor emission detected in the acceptor channel and the acceptor emission caused by a direct excitation.

To take into account such contributions, far more complex measuring methods must be used [31] though, in the end, new noise terms could be introduced. To avoid all these cumbersome procedures, we followed a more straight way carefully choosing either the donor excitation wavelength and the acceptor emission channel bandwidth.

Figure 1A shows the absorption curves of Alexa Fluor 488 (dashed line) and Alexa Fluor 568 (dotted line) along with their absorbance ratio (continuous line). Using the Ar laser line at 458 nm as the donor excitation wavelength, the donor/acceptor absorption ratio is at its maximum thus satisfactorily facing the trade off between an efficient excitation of the donor while keeping the acceptor absorption level at a minimum. In this way the spectral bleed-through of the acceptor emission caused by a direct excitation will be negligible.

Figure 1B shows the emission characteristics of the two fluorophores. The dotted and dashed curves represent the emission signal of Alexa Fluor 568 and Alexa Fluor 488 respectively, integrated over a bandwidth spanning from λ to 750 nm. The third plot (continuous line) represents their ratio. Choosing an emission channel from 650 nm to 750 nm, the detected acceptor fluorescence will be about two orders of magnitude higher than the donor one while suffering an acceptable reduction to 24% of the total emission. This is a reasonable tradeoff between a low donor fluorescence spectral bleed-through and a still good signal from the acceptor.

Once set up these experimental parameters, the approximated formula (1) was safely used for a fast evaluation of FRET efficiency.

To check whether an acceptor SE signal was actually present, confocal λ-stacks images were acquired from double stained samples excited with the Ar laser line at 458 nm (donor excitation) and the resulting total emission spectrum was obtained.

Confocal 3D Z-stacks images of I_{AD} and I_{AA} were then taken by sequential acquisitions of the Alexa Fluor 568 fluorescence once excited by the laser lines at 458 nm and 543 nm respectively. FRET efficiency was calculated by using equation (1) for each one of the Z-stacks and then Z-projected onto a single 'extended focus' pseudocolor image.

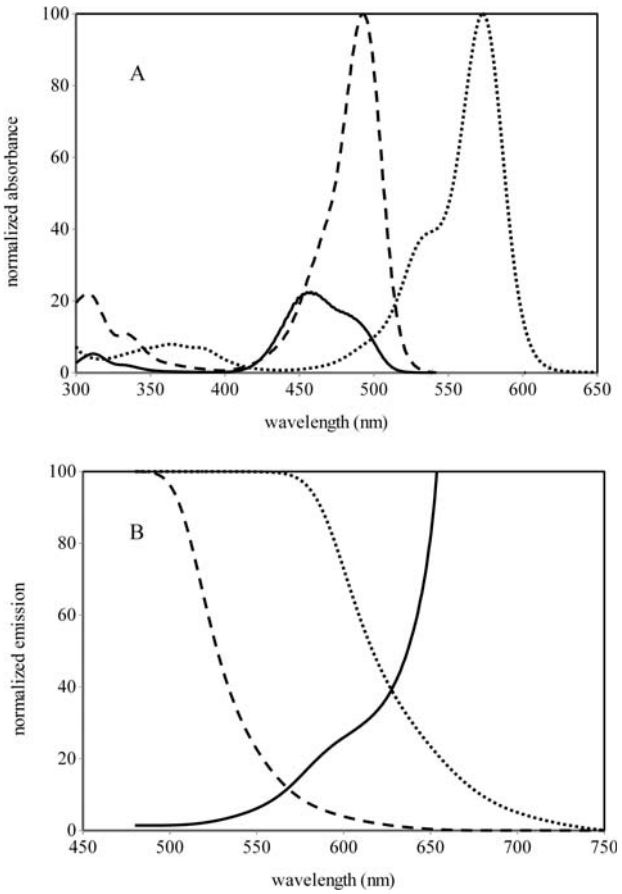

Figure 1 (**A**) Absorption spectra of the donor dye, Alexa Fluor 488 (dashed line), the acceptor dye Alexa Fluor 568 (dotted line), and donor-acceptor ratio (continuous line); (**B**) emission of Alexa Fluor 568 (dotted line) and Alexa Fluor 488 (dashed line), integrated over a bandwidth spanning from λ to 750 nm, and acceptor-donor emission ratio (continuous line).

It was also verified that spectral bleed-through contributions of donor and acceptor control samples were actually lower than the background noise level.

2.6 *Hyperspectral FLIM-FRET*

Our apparatus was a PCM2000 confocal laser scanning unit attached to a TE2000-U inverted optical microscope (CLSM); a CFI Planapo 60X/1.4 NA oil immersion objective was used for the measurements (Nikon Corp., Tokyo, Japan). The excitation light source was an ultrafast laser system made up of a Mira 900F mode-locked Ti:Sapphire oscillator pumped by a 5 W Verdi V5 (Coherent Inc., USA). The Ti:Sapphire output, tuned at 800 nm, was coupled by an aspheric lens (L) into a 30 cm long microstructured optical fibre (MOF) (NL-1.7-670, Crystal Fibre,) to produce a pulsed broadband supercontinuum (SC) radiation. A Faraday isolator (F) avoided back reflections into the laser cavity and a half-wave plate $\lambda/2$ was used to adjust the beam polarization.

The SC spectral band spanned from 390 nm to 1500 nm. At the MOF output a monochromator (M) of a special axial design [32] was used to tune the excitation wavelength. A 10 nm FWHM bandwidth around 460 nm was chosen, according to the previous reasoning (Figure 1A). A better excitation selectivity of the donor dye was also the reason why we preferred this complex one-photon excitation configuration based on a SC source instead of the straightforward two-photon approach. In fact, the two-photon absorption spectra of Alexa Fluor 488, and Alexa Fluor 568 are highly overlapping [33] and an unwanted excitation of the acceptor would be highly probable.

A 505DCLP dichroic long-pass beamsplitter (Chroma Technology Corp., Bellows Falls, VT USA), inside the confocal scanning head, coupled the 460 nm excitation wavelength into the optical microscope.

At the fluorescence output a 3 mm thick long-pass OG515 barrier filter (Schott AG, Mainz, Germany) was used to block out the excitation radiation. The fluorescence signal, through one of the two fibre coupled output ports, was sent, as usual, to the confocal control unit PMT. The image was shown on the confocal display to monitor and select the observation field of view, while the fluorescence light at the other output port was delivered to the hyperspectral fluorescence lifetime detection system. The FLIM equipment was composed of an imaging spectrograph (FICS, Model 77442, Spectra-Physics) interfaced with a 16-Channel Photomultiplier Head (PML-16, Becker & Hickl GmbH, Berlin) spanning a wavelength range from 410 to 650 nm, with a 16 nm channel width. The PML-16 detector was an Hamamatsu R5900-L16 multianode PMT with a time resolution of 200 ps.

Each one of the 16 independent PMT channels operated in photon counting mode and their signals were sent to a Time-Correlated Single Photon Counting module (TCSPC) [34] (SPC-830, Becker & Hickl) which built up the photon distribution versus time and channel number (wavelength). At the Ti:Sapphire output, a beamsplitter (BS) was used to reflect part of the beam towards a fast photodiode (P) to pick up the temporal reference pulse for the sync input of the SPC-830 TCSPC module.

The FLIM equipment was controlled by its instrument software (SPCM). The integration time for each image was 240 s, to attain an appropriate photon statistics. Data analysis was then performed by the SPCImage software, fitting each donor experimental decay curve by either a mono-exponen-

tial function, for the sample transfected with the donor alone (donor control), or by a bi-exponential one, for samples with both donor and acceptor:

$$F_d(t) = a_t\, e^{-t/\tau_t} + a_d\, e^{-t/\tau_d} \quad (2)$$

The fast lifetime component (a_t, τ_t) refers to the quenched donor fraction, involved in FRET process, while the slow lifetime component (a_d, τ_d) represents the unquenched one (no FRET) typical of the donor alone (donor control). The amplitude coefficients a_t and a_d represented the percentage of donors interacting or not with the acceptors, respectively [35, 36].

The fitted value of the slow lifetime τ_d was checked to be in agreement with the donor control one. When the result of the fit was outside the correct range, the datum was discarded. This "a posteriori" monitor on this parameter was done in order to put some kind of constraint on the fit results and thus to gain a better evaluation of the other ones.

From the fitted parameters we calculated the mean lifetime τ_m, and the FRET efficiency E:

$$\tau_m = a_t\tau_t + a_d\tau_d \quad (3)$$

$$E = 1 - \tau_t/\tau_d \quad (4)$$

Hyperspectral FLIM allows to acquire the fluorescence decay in several wavelength bands simultaneously. When measuring FRET with FLIM, the decay behaviors of both the donor and the acceptor fluorescence can be acquired contemporaneously and separately. In this way, it is possible to verify that the decrease of the donor fluorescence intensity and lifetime corresponds to an increase of the acceptor emission [37].

The temporal behavior of the acceptor fluorescence can be fitted by using the following Eqs. [38–41]:

$$F_a(t) = -b_t\, e^{-t/\tau_t} + b_a\, e^{-t/\tau_a} \quad (5)$$

The first term describes the slow rise of the acceptor fluorescence due to the energy transfer from the donor, while the second term represents the typical decay of the acceptor alone. The ratio b_t/b_a should be 1 [39], but it could deviate from this value mainly because of the spectral bleed-through of the donor fluorescence into the acceptor emission channel, substantially lowering this figure. For a correct estimation of the true acceptor decay, the donor contribution should be subtracted. The percentage of the leakage into the acceptor channel was estimated from the donor control sample. Then, for each pixel of the acceptor FLIM image the right fraction of the donor decay curve measured in the donor emission channel was subtracted from the acceptor one, after suitable deconvolution procedures had been performed on the rough data by using the Instrument Response Functions (IRF) of the respective emission channels [38]. These computations were carried out by custom made algorithms developed in Labview (National Instruments, Austin TX, USA).

3. Results and discussion

We first evaluated the time course expression of Cx43 and Cdo during C2C12 myoblast differentiation using confocal immunofluorescence. We found that both the molecules displayed a similar expression pattern (Figure 2A–P); in fact, the levels of Cx43 and Cdo were low in undifferentiated myoblasts (Figure 2A, H), increased substantially in the early stages of differentiation (48 h), (Figure 2C, J), and gradually decreased in the later time points (Figure 2D, K).

Of interest, the addition to the cell culture of a pro-myogenic factor, S1P (1 μM), [5] greatly potentiated the expression of both Cx43 and Cdo at 24 h, resulting in a 3- and 2-fold increase of the two protein, respectively, as judged by confocal (Figure 2E, L, O, P) and Western blotting analysis (Figure 2Q, R). These latter data, while consistent with the role played by Cx43 in S1P-mediated in vitro myogenesis [19], provided the first evidence to suggest that, besides Cx43, also Cdo could be a crucial downstream target of the sphingolipid action in myogenesis.

The same pattern of regulation and temporal induction of Cx43 and Cdo during C2C12 cell differentiation, allowed us to hypothize the existence of a functional interaction between the two proteins. To address this point, we next performed co-localization studies on 3D confocal Z-stacks acquired from double stained samples. The results showed a partial co-localization of Cx43 and Cdo in undifferentiated myoblasts (PC ≈ 0.6); the scatter plot (Figure 3A) displayed, in fact, two separate clouds of pixel intensities: the first one was distributed near the green channel axis indicating a small amount of non co-localizing immunolabeled Cdo, while the second one was placed along the bisector axis attesting a full co-localization. After 48h of differentiation (Figure 3D, F), the pixel distribution gradually concentrated along the bisector line, suggesting that the increased expression of both Cx43 and Cdo (Figure 2) was associated with an increased co-localization (PC ≈ 8). As shown in Figure 3H the co-localization of the two proteins was concentrated at the sites of the cell-to-cell contacts. In the later stages of differentiation (72 h), in concomitance with the downregulation of Cx43 and Cdo (Figure 2), the levels of co-localization of the two proteins were reduced reaching the basal values (PC ≈ 6; Figure 3E, F).

We also found that the amount of co-localized proteins increased significantly by stimulation with

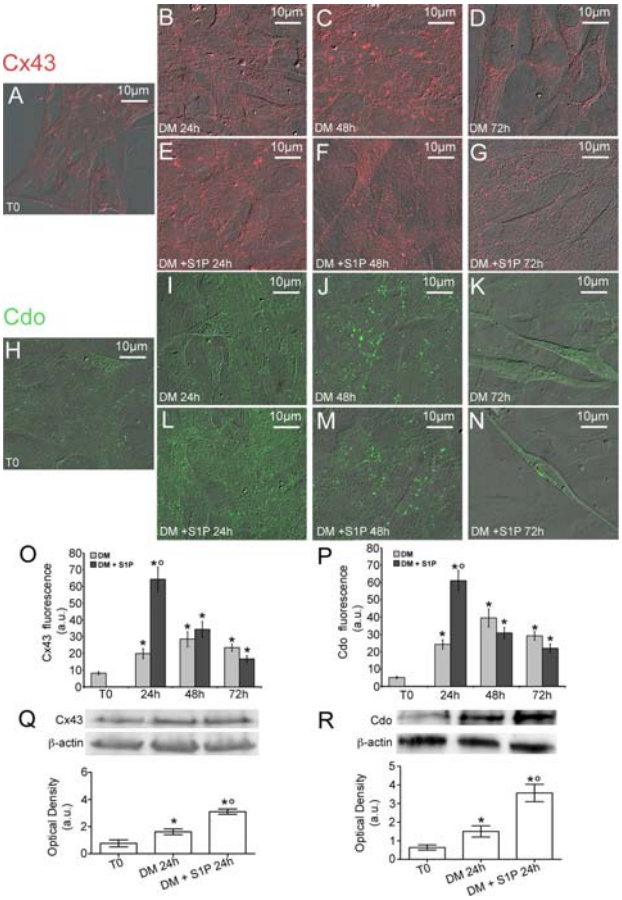

Figure 2 Time dependent expression of Cx43 (**A**–**G**) and Cdo (**H**–**N**) in differentiating C2C12 myoblasts. C2C12 cells cultured in the absence (**A**–**D**, **H**–**K**) or in the presence (**E**–**G**, **L**–**N**) of 1 μM S1P for 24 h (**B**, **E**, **I**, **L**), 48 h (**C**, **F**, **J**, **M**) and 72 h (**D**, **G**, **K**, **N**), were immunolabeled to reveal Cx43 (red) and Cdo (green) and then observed under confocal microscopy. Fluorescence and DIC images were merged to localize the immunostaining on the cell surface. (**O**, **P**) Time-course immunofluorescence analysis of Cx43 (**O**) and Cdo (**P**) in the indicated experimental conditions. (**Q**, **R**) Western blot analysis of Cx43 (**Q**), and Cdo (**R**) in untreated and 1 μM S1P treated C2C12 cells in basal conditions or after 24 H of culture. Data represent the results of at least three independent experiments with similar results, values are reported as average ± SD. $^{*}P < 0.01$ vs T0, $^{\circ}P < 0.01$ vs DM.

S1P (PC ≈ 7; Figure 3C, 3G) after 24 h of differentiation, and were reduced thereafter (PC ≈ 5, Figure 3G).

To verify whether the significant correlation between the spatial distributions of the two biomolecules found in the previous colocalization analysis was due to an actual interaction or not, SE-FRET analysis was carried out on C2C12 cells expressing the highest levels of Cx43 and Cdo (DM 48 h or DM + S1P 24 h).

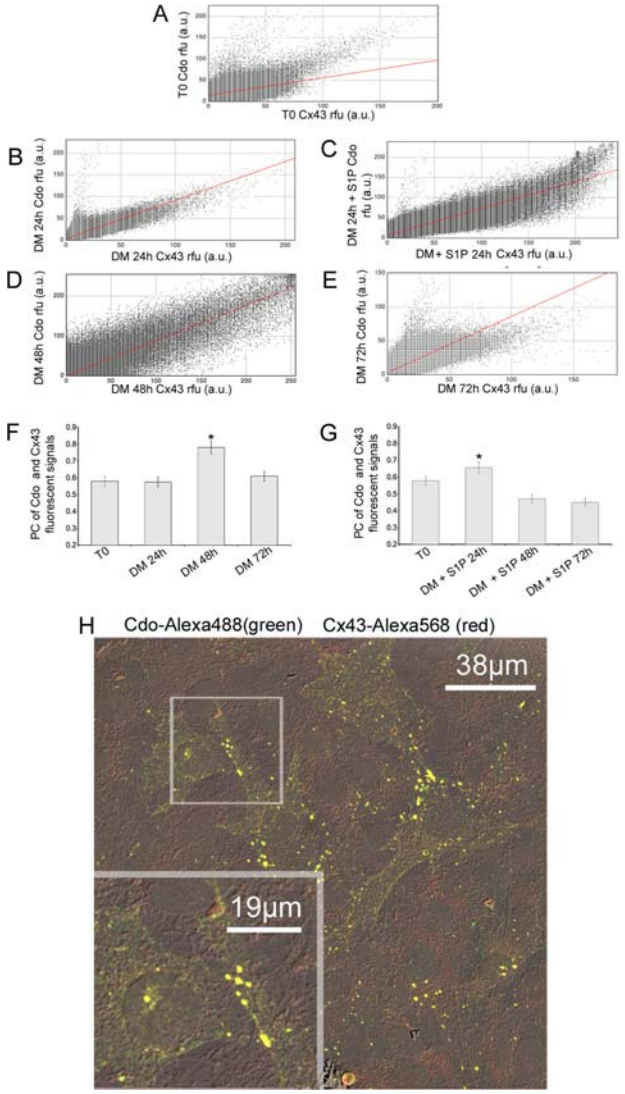

Figure 3 Colocalization of Cx43 and Cdo in differentiating C2C12 myoblasts. (**A**–**E**) scatterplots of fluorescent signals in C2C12 cells at T0 (**A**) and cultured for: 24 h (**B**), 48 h (**D**) and 72 h (**E**) in DM and 24 h (**C**) in DM + 1 μM S1P. (**F**, **G**) Time course evaluation of PC between immunolabeled Cdo (green) and Cx43 (red) fluorescence. PCs were calculated from confocal stacks of C2C12 cells cultured in the absence (**F**) or in the presence (**G**) of 1 μM S1P. All values are reported as average ± SD ($^{*}P < 0.01$ vs. T0). (**H**) Merge of fluorescence and DIC images in C2C12 cells cultured for 24 h in DM. Fluorescence of Cdo (green) and Cx43 (red) shows evident colocalization at discrete plasmamembrane sites, that are mainly localized in cell-cell contact surfaces (insert).

The emission spectrum of the donor (Cdo-Alexa Fluor 488), after excitation at $\lambda_{ex} = 458$ nm, showed a clear contribution of the acceptor (Cx43-Alexa Fluor 568) emission (SE) due to FRET (Figure 4A). Figure 4B shows the SE-FRET efficiency image in pseudocolor superposed with transmission DIC.

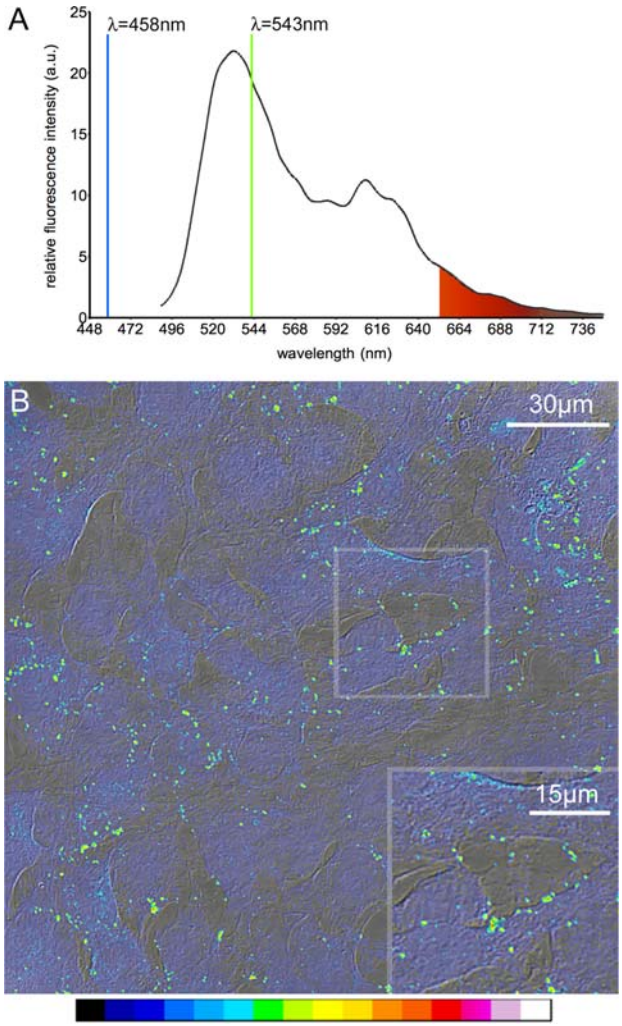

Figure 4 Sensitized Emission FRET. (**A**) Emission spectrum after excitation of the donor with $\lambda = 458$ nm. It shows a clear contribution of the acceptor emission (SE) due to FRET. The figure also shows the acceptor excitation wavelength $\lambda = 543$ nm and the emission spectral window: 650 nm–750 nm used for SE-FRET measurement. (**B**) Pseudocolor image of relative SE-FRET efficiency merged with the transmission DIC.

In order to provide a quantitative FRET analysis we performed hyperspectral FLIM measurements [24, 42]. The donor fluorescence decay in the absence of the acceptor (donor control sample) was well fitted by a mono-exponential function (Figure 5A, blue curve, $\chi^2 = 1.05$). This characteristic allowed a simpler FRET analysis devoid of rough approximations. In fact, a bi-exponential fitting for the donor fluorescence decay in the presence of the acceptor could have a straightforward interpretation (Figure 5A, red curve, $\chi^2 = 1$). The slow lifetime component was due to non-interacting (unquenched) donors while the fast component came from the interacting ones. The slow lifetime component was

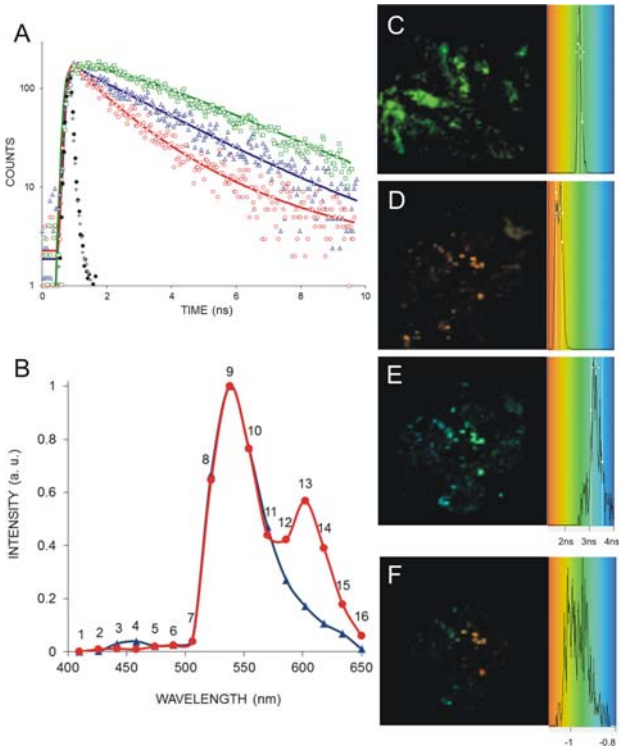

Figure 5 (**A**) (blue triangles) Donor fluorescence decay of the donor control sample; experimental data and mono-exponential fitting ($\tau_d = 2.612$ ns, $\chi^2 = 1.05$). (red circles) Experimental data and bi-exponential fitting ($a_t = 69.5\%$, $\tau_t = 1.122$ ns, $a_d = 30.5\%$, $\tau_d = 2.650$ ns, $\chi^2 = 1.0$) of the donor fluorescence decay in samples stained with both donor and acceptor (DM 48 h or DM + S1P 24 h). (green squares) Acceptor fluorescence decay due to FRET; experimental data and fitting according to Eq. (5) ($b_t = 46.5\%$, $b_a = 53.5\%$, $\tau_a = 3.124$ ns, $\chi^2 = 0.98$); the fast lifetime τ_t was held fixed at the corresponding value measured for the donor: $\tau_t = 1.122$ ns. The measured Instrument Response Functions at channel 9 (grey diamonds) and at channel 13 (black circles) are also shown. (**B**) Emission spectra ($\lambda_{ex} = 460$ nm) from 410 nm (channel 1) to 650 nm (channel 16) of the donor control sample (blue triangles) and the one of the sample with both fluorophores (red circles). The 16 PMT channels are indicated. Note the short-wavelength cutoff due to the OG515 emission filter. (**C**–**E**) FLIM pseudocolor images and lifetime histograms for: donor control sample lifetime τ_d (channel 9) (**C**), donor + acceptor lifetime τ_m (channel 9) (**D**) and acceptor lifetime τ_a (channel 13) (**E**). (**F**) Pseudocolor image of the ratio $-b_t/b_a$.

checked to be in agreement with the donor control one as specified in the previous section 2.6. The acceptor decay curve was fitted according to the model of Eq. (5) (Figure 5A, green curve, $\chi^2 = 0.98$).

Figure 5B shows the emission spectrum of the donor alone (donor control sample, blue curve), with a single peak centered around 538 nm (channel 9), and the one from a sample where both the donor

and the acceptor where present (DM 48 h or DM + S1P 24 h, red curve) which shows two different peaks: at 538 nm (donor emission) and 602 nm (channel 13), corresponding to the acceptor SE. The sharp short-wavelength cutoff was due to the presence of the OG515 emission filter which blocked part of the Alexa Fluor 488 fluorescence around its emission maximum (519 nm).

The FLIM image of the donor control sample, in the wavelength band corresponding to its maximum emission (channel 9), is shown in figure 5C in pseudocolors, along with the relative lifetimes histogram. The mean lifetime value was $\tau_d = 2650 \pm 80$ ps. Figure 5D shows the FLIM image of a double immunostained sample, again from channel 9; its mean lifetime was shortened, $\tau_m = 1830 \pm 150$ ps, whereas Figure 5E shows the same field of view of (D), in the wavelength band of the maximum emission of the acceptor (channel 13). This time the fluorescence decay was fitted using Eq. (5). The first term of the equation represents the slow rise of the acceptor fluorescence due to the energy transfer from the donor, the lifetime τ_t was then held fixed, in the fit, at the corresponding value measured for the donor: $\tau_t = 1.122$ ns. The FLIM image (E) shows the slow

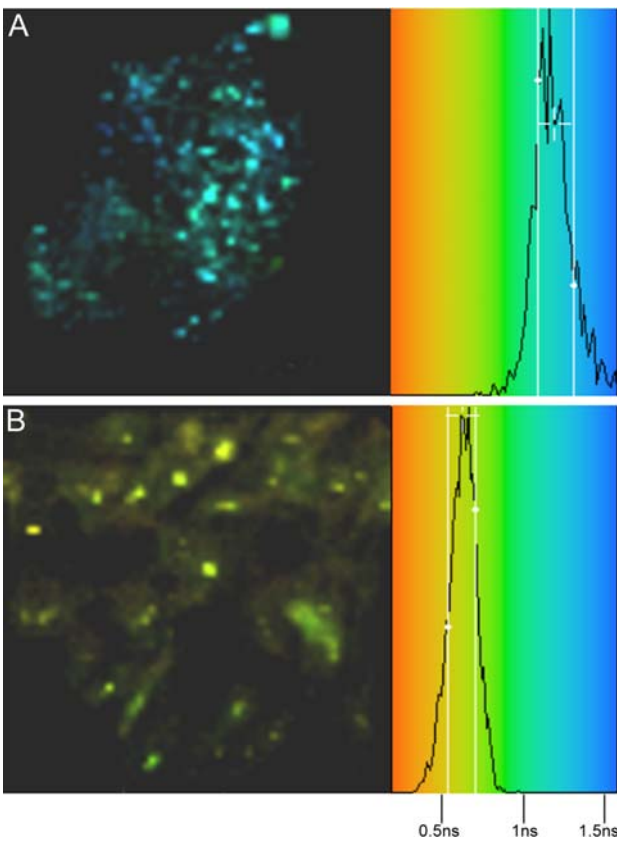

Figure 6 FLIM pseudocolor images of the fast component τ_t and the relative histograms for DM 48 h (**A**) and DM + S1P 24 h (**B**).

Table 2 FLIM-FRET statistics for samples cultured with and without S1P stimulation.

Sample	E_f	a_t (%)
DM 48 h	0.55 ± 0.07	62 ± 9
DM + S1P 24 h	0.75 ± 0.09	65 ± 6

lifetime τ_a while Figure 5F shows the ratio $-b_t/b_a$ which, according to the model, should be as close as possible to −1 [39]. Our result was in good agreement with the expected value.

Therefore, we can state that FRET has really occurred and Cdo and Cx43 interact at nanometric level.

We next measured samples stimulated with S1P in 24 h cultured myoblasts (DM + S1P 24 h) and compared the results with the samples without S1P stimulation in 48 h cultured myoblasts (DM 48 h). We have chosen again the samples with the maximum expression of the two proteins in order to have a better FLIM statistics.

Figure 6 shows the FLIM images and the relative lifetime histograms of the DM 48 h sample (A), and the DM + S1P 24 h sample (B).

We obtained the fast component τ_t of the fluorescent decay and the percentage of interacting donors a_t [30, 31] from each FLIM image from channel 9. We then averaged all these measurements and the mean value of their standard deviations was taken as the error. Using Eq. (4), we have then calculated the FRET efficiency.

Table 2 summarizes the results obtained for 10 different samples of DM + S1P 24 h and 6 different samples of DM 48 h.

The a_t amplitudes did not substantially vary in S1P-stimulated cells as compared to untreated ones in agreement with the confocal analysis showing that S1P was able to up-regulate the expression of both Cdo and Cx43. Moreover, we found that the FRET efficiency was higher in the cells stimulated with S1P, leading us to speculate that the sphingolipid could increase not only the expression of Cdo and Cx43 but also their interaction in our experimental protocol. This may be consistent with previous observations of our group and others showing that S1P affects the phosphorilation status and induces onformational changes of Cx43 protein [5, 19, 43, 44].

4. Conclusion

In conclusion, using multiple optical techniques, we have demonstrated that Cx43 and Cdo display the same pattern of regulation and temporal induction during in vitro myogenesis. These two proteins may physically interact with each other in differentiating

myoblasts, suggesting the existence of a functional interaction between adhesion and gap-junctional molecules at the site of cell-to-cell contacts. However, experiments are currently ongoing in our lab to address whether Cx43 and Cdo interact directly or through their associated proteins and to assess the functional consequence of this interaction on skeletal myoblast differentiation.

Acknowledgements F. Quercioli wishes to thank Ente Cassa di Risparmio di Firenze for the granted funding.

Author biographies Please see Supporting Information online.

References

[1] R. Yuste, Nat. Methods **2**, 902 (2005).
[2] R. S. Krauss, F. Cole, U. Gaio, G. Takaesu, W. Zhang, and J. S. Kang, J. Cell Sci. **118**, 2355 (2005).
[3] J. Dhawan and T. A. Rando, Trends Cell Biol. **15**, 666 (2005).
[4] M. Buckingham and D. Montarras, Curr. Opin. Genet. Dev. **18**, 330 (2008).
[5] E. Meacci, F. Bini, C. Sassoli, M. Martinesi, R. Squecco, F. Chellini, S. Zecchi-Orlandini, F. Francini, and L. Formigli, Cell. Mol. Life Sci. **67**, 4269 (2010).
[6] R. Vaz, G. G. Martins, S. Thorsteinsdóttir, and G. Rodrigues, Cell Tissue Res. **348**, 569–578 (2012).
[7] G. F. Weber, M. A. Bjerke, and D. W. DeSimone, Dev. Cell. **22**, 104 (2012).
[8] S. Yonemura, Curr. Opin. Cell Biol. **23**, 515 (2011).
[9] J. S. Kang, J. L. Feinleib, S. Knox, M. A. Ketteringham, and R. S. Krauss, Proc. Natl. Acad. Sci. **100**, 3989 (2003).
[10] G. Takaesu, J. S. Kang, G. U. Bae, M. J. Yi, C. M. Lee, E. P. Reddy, and R. S. Krauss, J. Cell Biol. **175**, 383 (2006).
[11] J. S. Kang, G. U. Bae, M. J. Yi, Y. J. Yang, J. E. Oh, G. Takaesu, Y. T. Zhou, B. C. Low, and R. S. Krauss, J. Cell Biol. **182**, 497 (2008).
[12] G. U. Bae, B. G. Kim, H. J. Lee, J. E. Oh, S. J. Lee, W. Zhang, R. S. Krauss, and J. S. Kang, Mol. and Cell. Biol. **15**, 4130 (2009).
[13] R. S. Krauss, Exp. Cell. Res. **316**, 3042 (2010).
[14] J. S. Kang, M. Gao, J. L. Feinleib, P. D. Cotter, S. N. Guadagno, and R. S. Krauss, J. Cell. Biol. **138**, 203 (1997).
[15] J. S. Kang, P. J. Mulieri, Y. Hu, L. Taliana, and R. S. Krauss, EMBO J. **21**, 114 (2002).
[16] D. E.Gutstein, F. Y. Liu, M. B. Meyers, A. Choo, and G. I. Fishman, J. Cell Sci. **116**, 875 (2003).
[17] C. M. Niessen, J. Invest. Dermatol. **127**, 2525 (2007).
[18] K. Willecke, J. Eiberger, J. Degen, D. Eckardt, A. Romualdi, M. Güldenagel, U. Deutsch, and G. Söhl, Biol. Chem. **383**, 725 (2002).
[19] R. Squecco, C. Sassoli, F. Nuti, M. Martinesi, F. Chellini, D. Nosi, S. Zecchi-Orlandini, F. Francini, L. Formigli, and E. Meacci, Mol. Biol. Of the Cell **17**, 4896 (2006).
[20] K. Boengler, R. Schulz, and G. Heusch. Heart **92**, 1724 (2006).
[21] P. Kameritsch, K. Pogoda, and U. Pohl, Biochim. Biophys. Acta [Epub ahead of print] (2011).
[22] J. R. Lakowicz, Principles of Fluorescence Spectroscopy, 3rd edn. (Springer, 2006).
[23] G. J. Kremers, D. W. Piston, and M. W. Davidson, http://www.microscopyu.com/articles/fluorescence/fret/fretintro.html.
[24] Dylan M. Owen, Egidijus Auksorius, Hugh B. Manning, Clifford B. Talbot, Pieter A. A. de Beule, Christopher Dunsby, Mark A. A. Neil, and Paul M. W. French, Optics Letters **32**, 3408 (2007).
[25] C. Biskup, T. Zimmer, L. Kelbauskas, B. Hoffmann, N. Klöcker, W. Becker, A. Bergmann, and K. Benndorf, Microscopy Research and Technique **70**, 442 (2007)
[26] S. S. Vogel, C. Thaler, and S. V. Koushik, Sci. STKE **331**, re2 (2006).
[27] S. Bolte and F. P. Cordelières, J. Microscopy **224**, 213 (2006).
[28] Y. Sun, H. Wallrabe, S. A. Seo, and A. Periasamy, Chemphyschem. **12**, 462 (2011).
[29] E. A. Jares-Erijman and T. M. Jovin, Curr. Opin. Chem. Biol. **10**, 409 (2006).
[30] J. van Rheenen, M. Langeslag, and K. Jalink, Biophys. J. **86**, 2517 (2004).
[31] G. W. Gordon, G. Berry, X. H. Liang, B. Levine, and B. Herman, Biophys J. **74**, 2702 (1998).
[32] R. Mercatelli, S. Soria, G. Molesini, F. Bianco, G. C. Righini, and F. Quercioli, Opt. Express **18**, 20505 (2010).
[33] Fluorescent Probes for Two-Photon Microscopy, in: Molecular Probes Handbook, A Guide to Fluorescent Probes and Labeling Technologies, edited by I. D. Johnson, M. T. Z. Spence (Live Technologies Corporation, 2010).
[34] W. Becker, A. Bergmann, M. A. Hink, K. Konig, K. Benndorf, and C. Biskup, Microsc. Res. Tech. **63**, 58 (2004).
[35] D. Llères, J. James, S. Swift, D. G. Norman, and A. I. Lamond, J. Cell Biol. **187**, 481 (2009).
[36] R. A. Bhat, M. Miklis, E. Schmelzer, P. Schulze-Lefert, and R. Panstruga, PNAS **102**, 3135 (2005).
[37] W. Becker, A. Bergmann, C. Biskup, T. Zimmer, N. Klöcker, and K. Benndorf, Proc. SPIE **4620**, 79 (2002).
[38] W. Becker, A. Bergmann, G. Biscotti, K. Koenig, I. Riemann, L. Kelbauskas, and C. Biskup, Proc. SPIE **5323**, 27 (2004).
[39] S. P. Laptenok, J. W. Borst, K. M. Mullen, I. H. M. van Stokkum, A. J. W. G. Visser, and H. van Amerongen, Phys. Chem. Chem. Phys. **12**, 7593 (2010).
[40] J. B. Birks, J. Phys. B: At. Mol. Phys. **1**, 946 (1968).
[41] Y. C. Chen and R. M. Clegg, J. Microsc. **244**, 21 (2011).
[42] A. Pietraszewska-Bogiel and T. W. Gadella, J. Microscopy **241**, 111 (2011).
[43] J. L. Solan and P. D. Lampe, Biochem. J. **419**, 261 (2009).
[44] M. Tencé, P. Ezan, E. Amigou, and C. Giaume, Cell Signal. **24**, 86 (2012).